PROCEEDINGS OF SCIENCE

Lattice QCD with overlap fermions at the example of non-leptonic kaon decays

Bjoern Walk* **and Hartmut Wittig**
Institut für Kernphysik, Johannes Gutenberg-Universität Mainz,
E-mail: bwalk@kph.uni-mainz.de, wittig@kph.uni-mainz.de

With the advent of Ginsparg-Wilson fermions problems involving chiral symmetry can be treated on the lattice with controllable error. One prominent solution to the Ginsparg-Wilson relation are overlap fermions. Unfortunately, simulations with chiral fermions are still extremely hard to simulate both in terms of computational demand and algorithmic reliability. In this proceedings, we present the experiences with our GPU-based implementation of overlap fermions. We show results on the computation of low-energy couplings for non-leptonic kaon decays using topological zero-mode wave functions.

31st International Symposium on Lattice Field Theory - LATTICE 2013
July 29 - August 3, 2013
Mainz, Germany

*Speaker.

PoS(LATTICE 2013)124

1. Introduction

The quantitative or even qualitative understanding of non-leptonic kaon decays, $K \to \pi\pi$, from first principles remains a formidable challenge despite decades of work. The main difficulty is that non-perturbative low-energy dynamics of the strong interaction play a significant role in these processes and it has turned out to be difficult to reduce the systematic errors of lattice computations to a tolerable level. This is because of the prohibitive cost of treating chiral symmetry, final state kinematics and physical quark masses on the lattice.

Instead of the direct computation of $K \to \pi\pi$ decay amplitudes, another approach is to determine, via lattice simulations, the low-energy constants (LECs) of the effective chiral weak Hamiltonian that describes these decays. This is done by matching lattice measurements of suitable correlation functions to the same correlation functions computed within chiral perturbation theory (χPT). A direct advantage of this procedure is that this matching does not necessitate physical kinematics or physical quark masses, as long as the regime of validity of χPT is reached. This however requires sufficiently large volumes and small quark masses.

The ordering in which the volume is increased and the quark masses are decreased can be chosen freely. When approaching the chiral limit first by decreasing the quark masses, the so-called ε-regime of χPT is reached, and in this kinematical regime it is possible to work out next-to-leading order corrections to χPT without introducing any more LECs than those at leading order.

At the same time, carrying out lattice simulations in the ε-regime is quite demanding. The Ginsparg-Wilson formulation of lattice fermions, which possess an exact chiral symmetry in the limit of vanishing quark masses, have made such simulations possible. The required computational cost, however, is still an order of magnitude higher than lattice simulations with for example the relatively cheap simulation of Wilson fermions.

In order to satisfy the increased demand for computational power, we utilize graphic processing units (GPUs) for our lattice simulation code. Ever since GPUs started to become highly parallelized computational units, the lattice community has tried to exploit their high amount of computational power[1, 2, 3]. With the advent of general programming frameworks for GPUs like NVIDIA CUDA, it is possible access the computational side of the GPU in a straightforward way. Details on our implementation of GPU-based lattice simulations can be found in [4] and [5].

In this proceedings, we concentrate on the reproduction of previously established results in order to verify our GPU-based implementation of our lattice simulation code. Primarily, we closely follow the work in [6], in which the rôle of the charm quark mass in $K \to \pi\pi$ was discussed based on a strategy proposed in [7]. We show results on the leading-order weak LECs in a theory with a light charm quark, that is in a four-flavour theory with an exact SU(4) chiral symmetry in the valence sector, which is also referred to as the GIM limit.

2. Low-energy couplings from zero-mode wave functions

In [8], the observables used for the matching between lattice simulation and χPT were three-point correlation functions of two left-handed currents and a weak operator. Here, we consider correlation functions of two pseudo-scalar densities and a weak operator. These correlators develop poles in $1/m^2$ in the ε-regime when evaluated in sectors of non-vanishing topological charge,

Lattice	β	V	$\lvert\nu\rvert$	$N_{\text{cfg}}^{\lvert\nu\rvert}$	x_0/a, y_0/a	am
A1	5.8458	16^4	1–5	288, 279, 279, 223, 159	5, 11	0.0015, 0.0025, 0.005

Table 1: The simulation parameters.

which is defined like in [9]. We will show that the residues of these poles are easier to compute numerically than the correlation function themselves, primarily, because certain propagators can be substituted by projectors to the zero-mode wave functions and need not to be computed explicitly.

2.1 Correlation functions in the fundamental theory and chiral perturbation theory

The weak Hamiltonian in the SU(4)-symmetric case, $m_{\text{u}} = m_{\text{d}} = m_{\text{s}} = m_{\text{c}} = m$, can be written as a linear combination of four-quark operators of the kind

$$O_1^{\pm} = [O_1]_{\text{rsuv}} \pm [O_1]_{\text{rsvu}}, \tag{2.1}$$

$$[O_1]_{\text{rsuv}} \equiv (\bar{\psi}_{\text{r}}\gamma_\mu P_- \tilde{\psi}_{\text{u}})(\bar{\psi}_{\text{s}}\gamma_\mu P_- \tilde{\psi}_{\text{v}}), \tag{2.2}$$

and a first order chiral expansion in the non-perturbative regime yields the low-energy couplings g_1^+ and g_1^-. See [6] for more details.

The task is then to match for the coefficients $g_1^{\pm}$ in the chiral limit by comparing lattice simulations with χPT predictions. The observable we use to carry out the matching in a finite volume are the bare three-point function in a fixed topological sector of charge ν,

$$A_\nu^{\pm}(x_0 - z_0, y_0 - z_0) \equiv -\lim_{m\to 0}(mV)^2 \int_{\boldsymbol{x}}\int_{\boldsymbol{y}} \langle \partial_{x_0} P(x) O_1^{\pm}(z) \partial_{y_0} P(y)\rangle_\nu, \tag{2.3}$$

with the bare pseudo-scalar density $P = i\bar{\Psi}\gamma_5\tilde{\Psi}$ and the quark mass m. We consider derivatives of the sources w.r.t. fixed time-slices x_0, y_0 in order to avoid contaminations from higher order LECs.

After carrying out the contractions and inserting the spectral representation of the quark propagator, the expansion of the three-point function in terms of zero-mode wave functions $v_i(x)$ for positive topological charge is then given by

$$\bar{A}_\nu \equiv \lim_{m\to 0}\frac{1}{L^3}\int_{\boldsymbol{z}} \langle \sum_{i=1}^{|\nu|} v_i^\dagger(z)\gamma_\mu \eta_i(z;x_0) \sum_{j=1}^{|\nu|} v_j^\dagger(z)\gamma_\mu \eta_j(z;y_0)\rangle_\nu, \tag{2.4}$$

$$\tilde{A}_\nu \equiv -\lim_{m\to 0}\frac{1}{L^3}\int_{\boldsymbol{z}} \langle \sum_{i,j=1}^{|\nu|} v_i^\dagger(z)\gamma_\mu \eta_j(z;y_0) v_j^\dagger(z)\gamma_\mu \eta_i(z;x_0)\rangle_\nu. \tag{2.5}$$

We have introduced an extended propagator $\eta_i(z;x_0) = \partial_{x_0}\int_{\boldsymbol{x}} P_{-\chi} S_m(z,x) P_\chi v_i(x)$, i.e. the inversion of the Dirac operator with a topological zero-mode as a source.

It is convenient to normalize these three-point functions with bare two-point functions of the pseudo-scalar density and the left-handed current, $L_0 = \bar{\Psi}\gamma_0 P_-\tilde{\Psi}$,

$$-iB_\nu(x_0 - z_0) = \lim_{m\to 0}(mV)\int_{\boldsymbol{x}} \langle \partial_{x_0} P(x) L_0(z)\rangle_\nu. \tag{2.6}$$

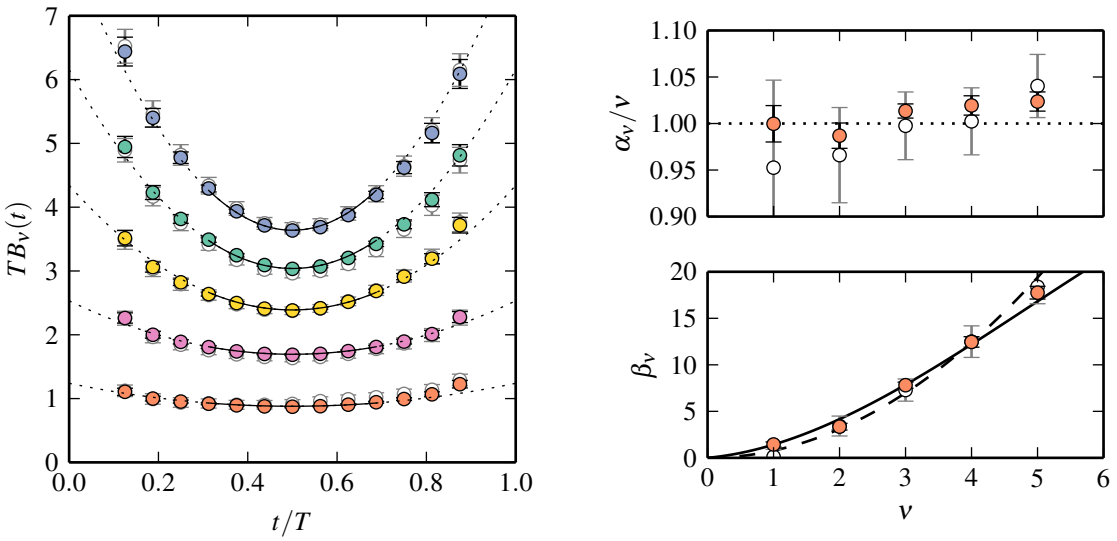

Figure 1: Left: The renormalized two-point function $TB_\nu(t)$ for the smallest quark mass $am = 0.0015$ and the fit to NLO predictions in the interval $\Delta t = 5a - 11a$. **Right:** The fit parameters α_ν, β_ν as a function of $|\nu|$. In the case for β_ν, the dashed line is the best NLO fit, the solid line is the best fit to NNLO predictions. In both cases open/full symbols correspond to data without/with LMA. Error bars are in most cases smaller than the symbol size.

Similar to the case of the three-point function, we can obtain the zero-mode expansion

$$B_\nu(x_0 - z_0) = \lim_{m\to 0} \frac{1}{L^3} \int_{\boldsymbol{z}} \langle \sum_{i=1}^{|\nu|} v_i^\dagger(z)\gamma_0\eta_i(z;x_0)\rangle_\nu . \tag{2.7}$$

This two-point function can be related through the non-singlet axial Ward identity to the two-point function of two pseudo-scalar densities, considered in [12], and we obtain an important relation

$$Z_A B_\nu(x_0 - z_0) = D_\nu(x_0 - z_0) \equiv \frac{1}{V}\int_{\boldsymbol{x},\boldsymbol{z}} \langle \sum_{i,j=1}^{|\nu|} v_j^\dagger(x)v_i(x)v_i^\dagger(z)v_j(z)\rangle_\nu . \tag{2.8}$$

On the right-hand side the limit $m \to 0$ has been taken analytically while it needs to be taken numerically on the left-hand side. Therefore, the Ward identity allows for a non-trivial test on our ability to approach the necessary limits in this procedure.

At next-to-leading order (NLO) chiral perturbation theory, the two-point function is predicted to have the following dependence on the topological charge

$$T\mathscr{B}_\nu(x_0 - z_0) = |\nu|\left\{1 + \frac{2\rho|\nu|}{(FL)^2} h_1(\tau_x)\right\}, \tag{2.9}$$

where $\tau_x \equiv (x_0 - z_0)/T$, $\rho \equiv T/L$ the aspect ratio and $2h_1(\tau) \equiv [(\tau \mod 1) - 1/2]^2 - 1/12$, while for the normalized three-point function we expect

$$\mathscr{R}_\nu^\pm = \frac{\bar{\mathscr{A}}_\nu(x_0 - z_0, y_0 - z_0) \pm \tilde{\mathscr{A}}_\nu(x_0 - z_0, y_0 - z_0)}{\mathscr{B}_\nu(x_0 - z_0)\mathscr{B}_\nu(y_0 - z_0)} = \left(1 \mp \frac{1}{|\nu|}\right)\left[1 \pm r_\pm(z_0)\right]. \tag{2.10}$$

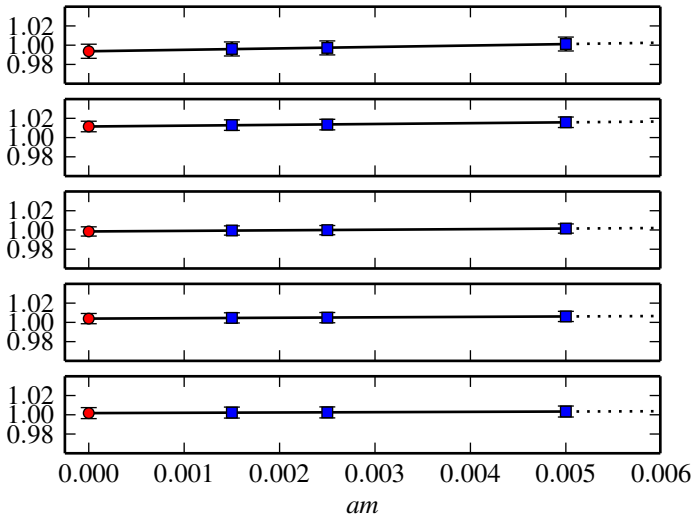

Figure 2: Chiral extrapolation on the time-averaged ratio $D_\nu(T)/B_\nu(t)$ normalized to $\hat{Z}_A = 1.710$ for the topological sectors $|\nu| = 1-5$. Where not visible, error bars are smaller than the symbol size.

The function $r_\pm(z_0)$ is a function of z_0 only and is independent on the topology ν, and can be evaluated numerically.

3. Numerical results

We have carried out simulations in the quenched approximations. In Tab. 1, we show the simulation parameters for a symmetric lattice with $T = L \simeq 2\,\mathrm{fm}$. The chiral quark propagator is computed on quenched background gauge configurations, using the Neuberger-Dirac operator with $s = 0.4$. A detailed overview of the numerical implementation can be found in [11]. We have also used low-mode averaging (LMA) as a technique to reduce statistical fluctuations of the signal of the correlation functions.

On the left side of Fig. 1, we show the results on the two-point function $B_\nu(t)$ (see Eq. (2.7)) in the topological sectors $|\nu| = 1-5$ at the lightest quark mass. Open symbols correspond to results without LMA while for the full symbols LMA has been used. There is a strong dependence on $|\nu|$, as expected from χPT. We have considered a two-parameter fit of the form $TB_\nu(t) = \alpha_\nu + 2\beta_\nu h_1(t/T)$, with h_1 given in Eq. (2.9). We have fitted the data in the time interval $\Delta t = 5a - 11a$ and linearly extrapolated the results of α_ν and β_ν to the zero mass limit.

On the right-hand side of Fig. 1, the results of α_ν and β_ν as a function of $|\nu|$ are given. In the case of α_ν, the NLO prediction $\alpha_\nu = |\nu|$ is extremely well reproduced. The prediction for β_ν depends on the value of F. The dashed line in the figure corresponds to a fit to the NLO prediction with F left as a free parameter. The best fit values are $FL = 1.60(8)$ with $\chi^2_{\mathrm{red}} = 4.6$. In order to take into account higher order chiral corrections, we take advantage of the Ward identity (cf. Eq. (2.8)) and consider a mid-point expansion of the form $TB_\nu(t) = \gamma_\nu + \delta_\nu(t/T - 1/2)^2$. For the dependence of δ_ν on the topological charge ν see [12]. The values for δ_ν agree with those for β_ν. Leaving F as a free parameter, the results of the fit for NNLO is $FL = 1.10(2)$ with $\chi^2_{\mathrm{red}} = 1.8$.

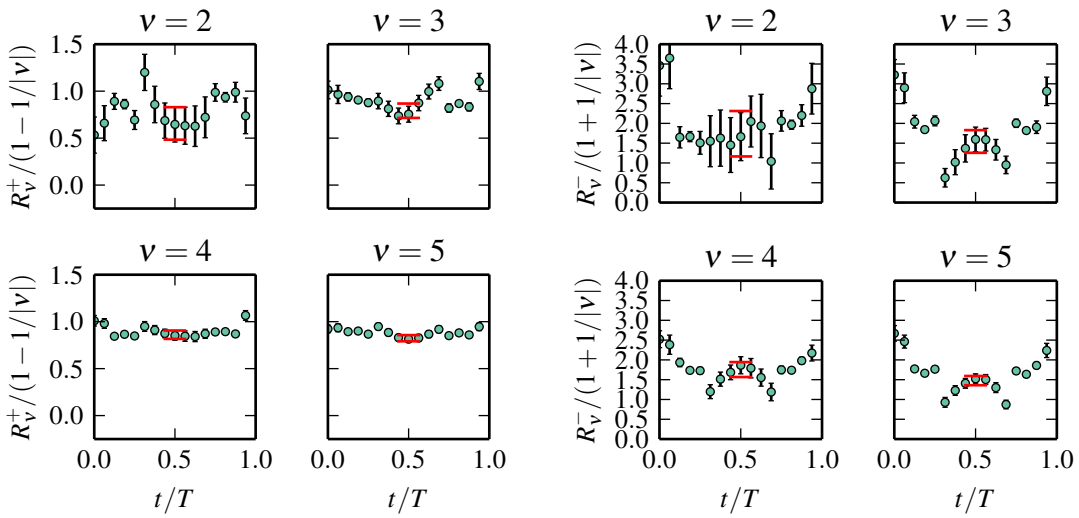

Figure 3: $R_\nu^\pm/(1\mp 1/|\nu|)$ in different topological sectors as a function of z_0/T for fixed $x_0 = 5$, $y_0 = 11$, at the smallest quark mass $am = 0.0015$. The horizontal lines represent the 1σ boundaries of the LO fit.

$\lvert\nu\rvert$	$[g_1^+]^{\text{bare}}$	$[g_1^-]^{\text{bare}}$	$[g_1^+ g_1^-]^{\text{bare}}$	$[g_1^-]^{\text{bare}}$
2	0.66(17)	1.73(57)	1.12(48)	1.70(48)
3	0.79(8)	1.54(29)	1.19(24)	1.51(32)
4	0.86(4)	1.75(19)	1.51(19)	1.76(22)
5	0.82(3)	1.47(12)	1.21(10)	1.48(19)
w.a. ($\lvert\nu\rvert > 2$)	0.83(3)	1.55(9)	1.27(8)	1.59(13)
χ^2_{red}	0.4	0.8	1.0	0.5

Table 2: Values of the bare low-energy couplings obtained from the LO fit in the time interval $|z_0| \leq a$.

As mentioned before, the Ward identity in Eq. (2.8) is a good test of the extrapolation $m \to 0$. In Fig. 2, we show the results for $Z_A \equiv D_\nu(t)/B_\nu(t)$ as a function of am in different topological sectors, normalized to the value $\hat{Z}_A = 1.710$ obtained for example in [13]. In the limit $m \to 0$, we expect the ratio to approach unity in all topological sectors, which is well reproduced by the data. From these results we can infer that the small residual extrapolation to zero quark mass is under good control.

In Fig. 3, we show the results for the bare ratios $R_\nu^\pm(x_0 - z_0, y_0 - z_0)/(1 \mp 1/|\nu|)$ as a function of $\tau = z_0/T$, at fixed $x_0 = 5$, $y_0 = 11$ for the smallest quark mass. From Eq. (2.10), we expect $R_\nu^\pm = [g_1^\pm]^{\text{bare}}(1 \mp 1/|\nu|)$ at LO, therefore fitting the data to a constant around $z_0 = 0$ is sufficient to extract the LECs $[g_1^\pm]^{\text{bare}}$. The 1σ boundaries of the fit are included in the figure and the numerical values are summarized in Tab. 2. We see a good agreement with the results from [6]

Especially for the ratio R_ν^-, NLO corrections are clearly visible. One possible strategy is to obtain $[g_1^-]^{\text{bare}}$ indirectly from $[g_1^+ g_1^-]^{\text{bare}}$ and $[g_1^+]^{\text{bare}}$. The first quantity is extracted from the product $R_\nu^+ R_\nu^-$, in which the NLO correction vanishes. Results have been summarized in the last two columns of Tab. 2. We see that the combined extraction and the individual extraction agree

with each other. We are working on a fit to the NLO predictions (cf. Eq. (2.10)), however, results were not yet available.

4. Conclusions and outlook

In this proceedings, we have shown results on the GPU-based computation of low-energy couplings for non-leptonic kaon decays using ratios of three-point functions of pseudo-scalar densities and a weak four-quark operator and two-point functions of pseudo-scalar densities and the left-handed current. We have concentrated on the reproduction of previously established results in order to verify our implementation. We see very good agreement for both predictions from χPT and the results established in [6]. We are fully confident that our GPU-based implementation is valid and can be used to extend the analysis to the case of a non-degenerate charm quark (outside the GIM limit). There, additional diagrams need to be computed in order to investigate the role of an active charm quark on the process $K \to \pi\pi$.

This work has been partially funded by the DFG via GK1581 and the "Forschungszentrum EMG". We are indebted to the "Center for Computational Sciences" in Mainz and the Helmholtz-Intitute Mainz for access to the GPU cluster on which simulations in this work were performed.

References

[1] G. I. Egri, Z. Fodor, C. Hoelbling, S. D. Katz, D. Nogradi and K. K. Szabo, Comput. Phys. Commun. **177** (2007) 631.

[2] K. Barros, R. Babich, R. Brower, M. A. Clark and C. Rebbi, PoS LATTICE **2008** (2008) 045 [arXiv:0810.5365 [hep-lat]].

[3] M. A. Clark, PoS **LATTICE2009** (2009) 003 [arXiv:0912.2268 [hep-lat]].

[4] B. Walk, H. Wittig, E. Dranischnikow and E. Schömer, PoS LATTICE **2010** (2010) 044 [arXiv:1010.5636 [hep-lat]].

[5] B. Walk, H. Wittig and E. Schömer, Eur. Phys. J. ST **210** (2012) 189.

[6] P. Hernandez, M. Laine, C. Pena, E. Torro, J. Wennekers and H. Wittig, JHEP **0805** (2008) 043

[7] L. Giusti, P. Hernandez, M. Laine, P. Weisz and H. Wittig, JHEP **0411** (2004) 016 [hep-lat/0407007].

[8] L. Giusti, P. Hernandez, M. Laine, C. Pena, J. Wennekers and H. Wittig, Phys. Rev. Lett. **98** (2007) 082003 [hep-ph/0607220].

[9] P. Hasenfratz, V. Laliena and F. Niedermayer, Phys. Lett. B **427** (1998) 125 [hep-lat/9801021].

[10] P. Dimopoulos, L. Giusti, P. Hernandez, F. Palombi, C. Pena, A. Vladikas, J. Wennekers and H. Wittig, Phys. Lett. B **641** (2006) 118 [hep-lat/0607028].

[11] L. Giusti, C. Hoelbling, M. Lüscher and H. Wittig, Comput. Phys. Commun. **153** (2003) 31 [hep-lat/0212012].

[12] L. Giusti, P. Hernandez, M. Laine, P. Weisz and H. Wittig, JHEP **0401** (2004) 003 [hep-lat/0312012].

[13] J. Wennekers and H. Wittig, JHEP **0509** (2005) 059 [hep-lat/0507026].